Preprint Title	Porous materials: microporosity induced by the shape and length of the pores
Authors	Leonid Titelman
Publication Date	30 Jul 2020
Article Type	Full Research Paper
Supporting Information File 1	Supporting information.xlsx; 38.5 KB
ORCID® iDs	Leonid Titelman - https://orcid.org/0000-0002-9891-0656

Beilstein J. Nanotechnol.

Porous materials: microporosity induced by the shape and length of the pores

Titelman L.

Full Research Paper

Department of Chemical Engineering, Ben-Gurion University of the Negev, P.O.B. 653, Beer Sheva, 8410501 Israel
Email: Titelman_leonid@hotmail.com

Postal: Shraga Rafaeli 1/6, Petah Tiqwa, 49064013 Israel

Keywords: Generalized parameter; Micropore; Molecular sieve; Pore length; Pore shape.

Abstract

There are insufficient parameters to explain the appearance of microporosity in porous materials. One of the parameters associated with micropores is the generalized pore shape factor F, which includes, as special cases, the known slit, circular and spherical model pore shapes. F covers the shapes between the slit (F = 2000) and spherical (F = 6000), as well as beyond. For the intermediate shape, one can estimate proportions of model motifs. The transition of the shape from one model to another is accompanied by the appearance of micropores (or vice versa); corresponding dependencies are given.

Nanotechnologies, such as self-assembly of ordered mesoporous materials (OMMs), the production of carbon OMMs as replicas of silica matrixes, supercapacitors made of carbon nanofibres (CNF), a hybrid CNF/MWCNT for use in lithium-ion batteries, carbon xerogels with Ni additive for storage of H_2, catalysis and others are discussed; they cover materials with F in the range 1,100 ÷ 32,600.

A pore surface length index L_{si} is proposed for any pore shape; it supplements the generalized parameters causing stresses, deformations and micropores. Using F and L_{si}, it was

discovered, that activated carbon, obtained as a replica of non-circular matrix of silica, behaves like a compressed spring, which, after removal of silica, expands and its pores become circular.

A concept of molecular sieving based on the shape of molecules is proposed and demonstrated by the example of lipase immobilization.

Application of the proposed parameters improves understanding of many published and new results.

Highlights

Change in pore shape and length causes microporosity

The carbon replica stretches and pore becomes circular after removing the silica matrix

A sieving concept based on the shape of molecules has been proposed and demonstrated.

Introduction

A certain size effect should be taken into account when evaluating the strength of a solid product, including nanoporous material. The statistical theory of strength explains this effect: the larger the body, the greater the likehood of defects arising under the action of the applied force.

In porous materials the expected defects were: first, part of the SBA-15 *micropores* [1], and then part of the intra-wall pores of OMMs [2]. The parameter representing the size was the ratio of the wall thickness ***t*** to the average pore diameter D_p.

As a parameter affecting the strength, ***t***/D is known from the works on cellular solids [3], thin silica films [4] and even cakes [5]. The ***t***/D_p represents dimensionless size in the *radial* direction of the pore; one of the ***goals*** of this work is to supplement it with a parameter acting in the *axial* direction.

The effect of a technological variable can be mentally replaced by a scheme of mechanical forces [6, 7]. Data on simultanious changes in both radial and axial dimensions under an action (influence) of some technological variable, being mentally replaced by mechanical force, will help to better understanding the properties of the material.

Micropores of materials play an important role in adsorption, separation and catalysis.

The microporous part of the total porosity depends on many processing parameters, in particular on the heating temperature and the preparation time of the material, as shown, for example, in Zukerman et al. [8].

It plays a significant role in many processes, for instance, it reduces the crystallization temperature of the active component in supported catalysts, makes crystals smaller and the catalyst more efficient [8].

One application of the microporous materials is the storage of hydrogen. It is known that an adsorbent for hydrogen storage should have a large surface area (S_{BET}) and a small pore size (D_p) [9].

For a circular pore, these two parameters were combined in the adsorbent *surface* length $L_s = S_{BET}/\pi D_p$ [2], but for non-circular pores this parameter *should be adjusted.*

L_s was combined with previously proposed adsorbate *volume* length L_v [6] into the parameter L_s/L_v, which, as was shown in [2], is equal to the ratio of the average pore diameter D_p to the pore hydraulic diameter D_h.

The expression $L_s/L_v = D_p/D_h$ (rouphness factor) was derived from formula for hydraulic diameter of circular pore [2], that is from D_h (nm) = 4000*V_p (cm^3/g)/S_{BET}(m^2/g). The factor 4000 should be changed to 2000 or 6000 for slit and spherical pore models, respectively [10, 11].

The $L_s/L_v = 1$ means that the surface is smooth and can serve as an *intrinsic* reference point of smooth surface [2].

There is a need for knowledge of intermediate (between slit and circular, circular and spherical) pore shapes, as well as shapes beyond the factors of 2000 and 6000. It can be expected

that the transition from one shape to another can be accompanied by stress and deformation that cause micropores: pits, cracks and crevices

Another detail of the shape that affects the efficiency of materials is the corrugation of pore walls [12], which should also be taken into account. Corrugation pipes to improve heat transfer are widely used in industry [13]. Thus, there is a need for a generalized factor that can cover all forms of pores.

The *main goal* of this article is to supplement the previously proposed [2] generalized texture parameters of porous materials with new ones and to detect some *unknown* properties or behavior of porous materials using the proposed parameters.

Result: new generalized parameters.

The generalized pore shape factor F.

Let D_{h4} denote the hydraulic diameter of the circular pore $D_{h4}= 4000V_p/S_{BET}$, that is, the diameter obtained from expression with a factor 4000. Accordingly, similar expressions with factors of 2000 and 6000 for slit and spherical pores will give D_{h2} and D_{h6}.

We will expand the formula for the hydraulic pore diameter for pores of *any* shape by introducing the factor F of any (i.e. general) pore shape as a factor for V_p/S_{BET} (in particular, F_2 = 2000, F_4 = 4000 and F_6 = 6000 - these are discrete factors of the slit, circular and spherical geometric shapes, respectively).

$$D_h = FV_p/S_{BET} \quad \text{..... 1.}$$

In turn, the average value of F can be obtained using the average pore diameter D_p found from some adsorption model, namely

$$F = D_pS_{BET}/V_p \quad \text{.....2.}$$

A similar expression was proposed in the field of cements [14], but without any connection with rouphness and microporosity. F gives a *continious series* of pore shapes. In particular, formula (2) allows us to estimate how close the real average pore shape is to the known simplest regular geometric shapes (with smooth surfaces [2]): slit, circular and spherical.

The rouphness and shape of the pores are closely related: $D_p/D_{h2} = F/F_2$, $D_p/D_{h4} = F/F_4$ and $D_p/D_{h6} = F/F_6$. The closer the ratio to unity, the closer the pores shape to one of the mentioned regular geometries, and the surface to smooth; the farther the ratios from unity, the more the pore shape becomes transitional from one regular shape to the neighboring one and the more the surface becomes rough.

One can imagine the transition of the slip pores into cylindrical as a transition of a smooth roofing panel to corrugate. That is, the *transition of shapes is accompanied by a change* in r*oughness* (and vice versa).

The difference between F of the slit and circular, circular and spherical shapes is 2000, so for the intermediate shape we can estimate the proportions (%) of the motives of each of the neighboring (slit and circular, circular and spherical) shapes. For example, pores with F = 2500 have 100*(2500-2000)/2000 % = 25% circular and 100*(4000-2500)/2000 % = 75% flat surfaces (motifs).

Pore surface length index $L_{si} = S_{BET}/D_p$.

As mentioned above, S_{BET} and D_p were combined in the surface length $L_s = S_{BET}/\pi D_p$ [2] for the circular pore. For the non-circular pores this parameter should be adjusted. Excluding π, the S_{BET}/D_p ratio can be ranked as one of the generalized texture parameters (GTP) of any porous material. Its change induces stress and strain in the porous material in the axial direction. We call it the *pore surface length index and denote L_{si}*.

Changes in both the axial dimension of $L_{si} = S_{BET}/D_p$ and the radial dimension of D_p itself provide additional information about the material. Simultanios axial and radial tension of the material under the action of a force (or technological parameter) may indicate its behavior similar to *auxetic material* [6]. You can also expect that a change in pore length will affect the shape of the pores and the proportion of micropores.

The t/D_p ratio as a generalized parameter.

The t/D_p ratio as a parameter related to the strength of materials is known in various fields [1, 3, 4, 5]. The appearance of F allows us to transfer t/Dp to the rank of a dimensionless *generalized* texture parameter (GTP). Dividing V_w/V_p (GTP-1, [6]) into D_p/D_h (GTP-2, [2]) and F, where $V_w = S_{BET}*t$ and $D_h = FV_p/S_{BET}$, we obtain (t/D_p). In other words, dividing one GTP into two others gives another generalized texture parameter, which we will denote as GTP-4. Thus, t/D_p can be considered not only as a parameter that causes stresses, but also as an ordinary texture parameter indicating the nuances of the formation of OMM, regardless of the stress state of the material.

Range of pore shapes.

To track the effect of processing variables on pore shape, let's start with the data of **Putz** et al. [15]. They synthesized 18 samples of MCM-41 by hydrolysis of TEOS in water and a mixture of water with 2-methoxyethanol. Technological variables were: catalyst (either NH_3 or NaOH), template (CTAB, DTAB or a mixture thereof), post-synthesis heating temperatures (^oC) and time (hours) (60°C-9 h, 500°C-6 h, 700°C-6 h). The name of the sample is made up of preparation conditions, for example CTAB-NH3-60. A combination of NaOH with 700°C has been reported to result in a loss of ordered structure.

The texture parameters S_{BET}, V_p and D_p were presented. We added shape factors F and length indices $L_{si.}$ The F range was *1280 ÷ 6126*, that is, the F series ranged from less than 2000 (the shape of the slit model) to more than 6000 (the shape of the spherical model).

Sorting data by F as a key you can select processing variables that provide the desired pore shape. Sequential data sorting by template, catalyst, and temperature as keys shows that temperature has the most pronounced effect on pore shape: serial samples heated at 60, 500 and 700ºC have averaged F values: 1891, 4868 and 2849, respectively.

All samples heated at 60°C have a disordered (apparently not yet formed) structure, what can be concluded because of the very low L_{si}. Data sorting by L_{si} as a key divides the samples into 2 series: 10 with short (L_{si} = 1.3 ÷ 10.7) and 8 with long (L_{si} = 224 ÷ 524.8) pores.

The mentioned series of NaOH-700ºC (3 samples) relates to short channels and has F ≈ 2000; therefore factor 2000 can indicate not only a split shape, but also a disordered structure.

The following study demonstrates high values of F. **Moyseowisz** et al. [16] manufactured carbon nanofibre (CNF) supercapacitors. Carbon nanofibers form unique nanostructures depending on the angle of inclination of graphene layers to the fiber axis.

Three structural types of CNF were studied: herringbone HCNF1- from Ni/Al_2O_3 + methane, HCNF2 - from the same catalyst + propane and platelets (PCNF), as well tubular CNF; in tubular CNFs graphene layers are parallel to the filament.

Two samples of CNTs were made: dried (CNT) and calcined at 450°C (CNT_{450}). "Among the studied CNFs, the highest capacitance value was obtained for the *platelet-type* CNFs; tubular CNFs exhibited the lowest capacitance value" [16]. The average values of pore diameter D_{av} (Table 1) were calculated by us as arithmetic mean of the diameters of the D_{pTEM} interval measured by the uthors using the TEM method [16]. The F and Lsi were added to the original data (Table 1).

Table 1: CNF and CNT pore shape test. Source data ($D_{p\,TEM}$, S_{BET} and V_p) from Moyseowisz et.al. [16].

Sample	Model	D_{pTEM},	D_{av},	S_{BET},	V_p,	F	L_{si}
		nm	nm	cm^2/g	cm^3/g	---	m2/(g*nm)
HCNF1	herringbone	20 - 60	40	150	0.417	14388	1.19
HCNF2	herringbone	15- 40	27.5	223	0.442	13874	2.58
PCNF	platelet	20 - 40	30	251	0.486	15494	2.66
CNT	tubular	10 - 20	15	296	0.805	5516	6.28
CNT_{450}	tubular	< 20	15	380	0.918	6209	8.07

D_{pTEM} – pore diameter, TEM method; D_{av} – mean value of D_{pTEM}, S_{BET} and Vp – total pore surface area and volume; F – pore shape factor, $L_{si} = S_{BET}/Dp$ - pore surface length index.

From the data of tubular CNTs it is seen that the spherical shape model (F = 6000) is the most suitable for them, but according to synthesis procedure they are tubular. We suggest that they are corrugated long circular pores.

Annealing CNT at 450°C makes it slightly more corrugated. F-s of CNF, created by graphene layers, are 2-3 times higher as CNT; they are wider (D_{av}) and shorter then CNT-s. The shape factor F = 15494 of platelet CNF is the highest. Thus, in this case the *highest capacity corresponds to the highest shape factor*.

The following example demonstrates shape transitions. **Jeong** et al. [17] reported the production of mesoporous (high V_{me}) CNFs from corn starch reinforced by MWCNT for use this hybrid in lithium-ion batteries. In addition to regular pore parameters, they presented both micropore and mesopore volumes V_{mi}, V_{me}. We hypothesized that in such a hybrid, the V_{mi}/V_{me} ratio may be related to the shape of the pores.

In the work, firstly, two CNF samples were prepared by carbonization of starch at 700 and 1400°C (Supporting Information File 1, in short SI-1, table S1-1). The pore shape factor in both samples was F ≈ 4000, which indicates a circular pore with a smooth surface.

Indeed, the authors report a smooth surface, but indicate the shape of the pores as a "more stable ladder configuration". An increase in temperature practically did not change the pore shape

and smooth surface of SNF, despite a sharp decrease in both the pore surface length index L_{si} and micropore volume V_{mi}, what, by the way, says about their connection. The SNF-700 was chosen by the authors [17] for the following experiments; it contains many micropores, but a small number of mesopores (V_{mi}/V_{me} = 6.7).

A hybrid CNF-700/CNT sample was activated (etched) by CO_2 at 800^{o}C for 15, 30, 45 and 60 min. Sample "Before" (before activation) was mainly microporous (V_{mi}/V_{me} =21). Carbon etching leads to an increase in the pore diameter Dp in direct proportion to the etching time over its entire range (SI-1, Fig. S1-2).

After 15 min of etching, all parameters increased, especially S_{BET}. We can see the simultanious expansion of the pore walls in both radial and axial directions, which is typical for a *material with a positive Poisson number (auxetic material)* [6]. The authors' idea [17] about the ladder construction of the material seems realistic : the steps rotate, mesopores appear (V_{mi}/V_{me} = 3), F becomes 6345, that is, with spherical surface areas. (Another model that comes to mind is the mesh: the filaments sometimes converge, leaving micropores, and then diverge, forming mesopores).

Steps after 15 min show the inverse proportional dependens of S_{BET} (SI-1, Fig. S1-1), L_{si} (SI-1, Fig. S1-3) and V_p (SI-1, Fig. S1-4) by activation time. F behaves differently: it increases from 3923 to 11537 (surface corrugation), but then decreases to 8092 (SI-2, Table S2-3 and Fig. S2-5).

The (SI-1, Fig.S1-5) shows that there is a certain critical temperature between 45 and 60^{o}C, starting from which the pore surface of the CNF/CNT hybrid material begins to smooth out. So, CNT-45m is a "critical" sample. This figure demonstrates the important property of F as a generalized parameter; F *divides the* samples into groups with some close or similar properties. From (SI-1, Table S1-2) it can be seen that materials having the same F ≈ 8000: CNT-30m and CNT- 60m are very different in S_{BET}, V_p and D_p, however V_{mi}/V_{me} (Fig. 1 below) makes their similar. Please note that the most effecient battery sample CNT-30m (F = 7527) has equal volumes of micro – and mesopores (V_{mi}/V_{me} = 1) (perhaps that makes it the best).

After 45 min activation (the sample CNT-45m, F = 11537), the micropores volume remaines the same as after 30 min, but the mesopores dissapear (the stairs may turn into a herringbone); after the last 15 min (sample CNT-60m), the mesopores appear again (0.19 cm^3/g), but the micropores dissapear (stairs return). Fig.1 shows how F separates the samples.

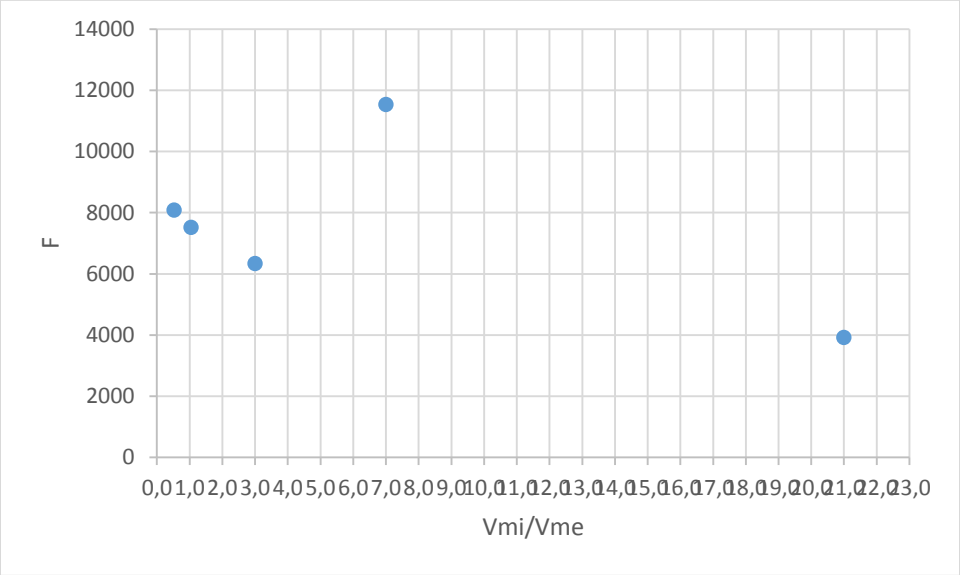

Fig.1: F vs. V_{mi}/V_{me}. Based on data from Jeong et al. [17].

Excluding the unactivated sample ("before", F = 3923) and the "critical" (F = 11537) sample, we obtain an inversely proportional dependence of F on the dimensionless V_{mi}/V_{me}.

Zubizarreta et al. [18] prepared carbon *xerogels* doped with Ni for H_2 storage. Two series of xerogel samples with an average mesopore size of 45 nm (a series of 4 samples) and 16 nm (another series of 4 saamples) were chemically activated, oxidised by HNO_3 and impregnated with Ni. Texture parameters are given: S_{BET}, V_p, $V_{<2\ nm}$ (by N_2) and $V_{\leq 1\ nm}$ (by CO_2).

Carbon should provide both good dispersion of Ni along the surface area during Ni impregnation and conditions for H_2 spillover during its adsorption. We supposed that micropores of different sizes are responsible for the capture of Ni and H_2.

The presented sample with the highest adsorption capacity had a diameter of 16 nm, was oxidized with nitric acid and doped with nickel. We calculated F, L_{si}, $V_{<2\ nm}/S_{BET}$ and $V_{\leq 1\ nm}/S_{BET}$ ratios; the averaged values and their standard deviations whithin the series are given in the table 2

Table 2. Some texture properties of Ni-doped carbon xerogels. Based on data from Zubizarreta et al. [18]

D_p, nm	L_{si} average, $m^2/(g*nm)$ (STD, %)	F average (STD, %)	$V_{<2\ nm}/S_{BET}$, cm^3/m^2, (STD, %)	$V_{\leq 1}$ nm/S_{BET}, cm^3/m^2, (STD, %)
16	109 (5.7)	16123 (10.2)	0.000417 (11.6)	0.000256 (16.0)
45	36 (5.3)	32635 (12.2)	0.000415 (4.4)	0.000277 (5.3)

D_p – average pore diameter, $L_{si} = S_{BET}/D_p$ – pore surface length index, $F = D_pS_{BET}/V_p$ – pore shape factor, $V_{<2\ nm}$, $V_{\leq 1\ nm}$ – volumes of pores with size < 2 nm or ≤1 nm respectively.

It folows from Table 2 that the best sample (D_p = 16 nm) , has pores 3 times longer (L_{si}) and 2 times less rough (F), but the values of the volumes of micropores per m^2 of surface area are the same with D = 45 nm. $V_{<2\ nm}/S_{BET}$ does not depend not only on D_p, but also on the conditions of xerogels processing.

Thus, we examined cases with F from 1300 to 32650.

Sieving based on the shape of molecules

(as opposed to sieving based on the size of molecules).

We assumed that in the case of complex probe molecules, the shape of the pores of the adsorbent can play the role of a sieve for the separation of molecules in accordance with their shape.

Serra et al. [19] studied lipase immobilisation in two OMM series: channel-like (MCM-41, SBA-15, Me-SBA-15, KIT-6 and Me-KIT-6) and cage-like (SBA-16, Me-SBA-16, FDU-12 and Me-FDU-12). In both series, a sample of SA- amorphous mesoporous silica with largest pore diameter (27.9 nm) and disordered structure was included as a reference point; it provides a highest load (45 mg/g) and, according to our calculations, had close to circular pore shape (F = 3152).

From both series, we select samples with a *close* average pore diameter (to exclude the effect of size) and a similar surface chemistry (unmethylated, i.e without "Me") namely namely (in ascending uptake) SBA-16, FDU-12, KIT-6 and SBA-15 (Fig. 2).

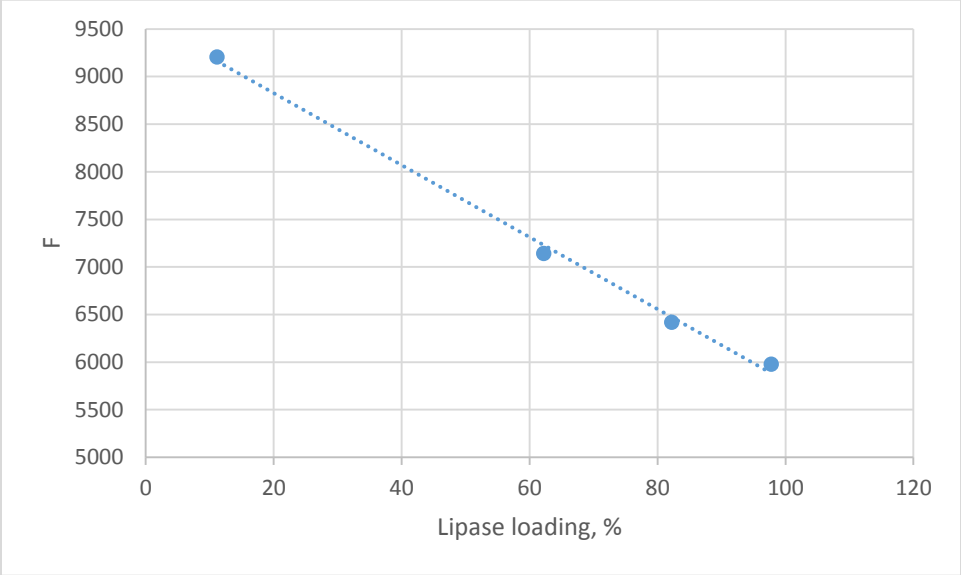

Fig. 2: Lipase loading,%, depending on the pore shape factor F. Materials, placed on an ascending loading: SBA-16, FDU-12, KIT- 6 and SBA-15. Based on data from Serra et al. [19].

Figure 2 shows that the more complex the shape of the sorbent (the larger the F value), the less lipase can enter the pores. For lipase, as a probe medium, these sorbents are molecular shape sieves.

The effectiveness of chemical reactions and the shape of the pores.

Landau et al. [20] showed the effect of the content of active sulfated tetragonal ZrO_2 in the SBA-15 host on: i) the yield of MTBE in the condensation reaction of t-BuOH and MeOH and ii) the conversion of isopropanol in iso-PrOH (dehydration reaction) (table 3). A 1.24-fold increase in the ZrO_2 content increased the reaction efficiency by 1.45 (1.43) times. Now the parameter F has been added to these data (table 3).

It can be seen that the increase in the catalyst efficiency can be explained not only by an increase in the mass of ZrO_2%, but also by an increase in F from 3058 to 4032. As a result, the ZrO_2 islands coalesce into a continuous circular surface, and ZrO_2 is better dispersed. The ratio $F_2/F_1 = 1.32$ is even closer to the ratio of conversion degrees (in %), i.e. 1.45 (1.43), than the ratio of ZrO_2 contents (1.24), i.e. ZrO_2 influences not only by its mass but also by changing the pore shape. In this case, the best pore shape is circular.

Table 3: The effect of parameter F on the activity of the catalyst SO_4/ZrO_2/SBA-15 in two reactions. Based on data of Landau et al. [20].

# of sample	Sample	ZrO_2 content, wt%	MTBE yield, wt.%	Isopropanol conversion, wt. %	F
1	SO_4/48%ZrO_2/SBA	48.1	32.3	9.2	3058
2	SO_4/60%ZrO_2/SBA	59.8	46.7	13.2	4032
Ratio 2/1	---	1.24	1.45	1.43	1.32

$F = D_pS_{BET}/V_p$ – pore shape factor

Discussion.

The creation of microporosity

Th. **Pagketanang** et al. [21] prepared activated carbon (AC) as a capacitor electrode from shells of rubber seeds by activation with KOH, washing with water and calcining in a stream of N_2 at 700, 800 and 900°C. Texture properties the both original and calculated by us F, L_{si} and V_{mi}/V_p are given in the table 4.

Table 4: Texture properties of activated carbon calcined at different temperatures. Based on data from Pagketanang et al. [21].

T	AC Yield,	S_{BET},	V_p,	D_p,	Lsi,	F	V_{mi}/V_p
oC	%	m^2/g	cm^3/g	nm	(m^2/g*nm)	---	%

700	27.52	429	0.201	2.165	198	4621	80.6
800	22.89	528	0.221	1.18	447	2819	90.0
900	20.83	620	0.284	0.95	653	2074	93.3

T – calcination temperature, AC – activated carbon, S_{BET} – total surface area, V_p – total pore volume, Lsi = S_{BET}/D_p – surface lenghth index, V_{mi} – micropore volume, D_p – average pore diameter, $F = D_pS_{BET}/V_p$ – pore shape factor.

Table 4 shows that an increase in the calcination temperature leads to a decrease in the diameter D_p, but the pore length index L_{si} increases; induced stresses cause an increase in the proportion of micropores in the total pore volume and the transition of the pore shape from circular to slit. The AC yield is direct proportional to the pore shape factor (not shown); micropore volume (%) is inversely proportional to F (*see graphical abstract*).

The ratio $V_{<2\ nm}/S_{BET}$ average value is 0.0004 cm^3/m^2 (STD - 7.4%).

From the graph (not shown) of the effect of the calcination temperature T on F (direct proportionality), it can be seen that T ≈ 740°C provides a circular pore shape (F = 4000), which, in turn, corresponds to V_{mi} = 84% and pore size 1.8 nm.

Silica SBA-15 is often used as a matrix in AC synthesis. **Zukerman** et al. [8] synthesized 2 samples of SBA-15, differing in the hydrothermal treatment time of the reaction mixture: 1 and 3 days. The V_{mi} fractions were 14.2 and 6.7%, our calculated Fs were 6233 and 4993, respectively; that is, after 1 day heating, the pore shape was spherical, but an additional treatment for 2 days led to the transformation of ≈ 50% of the surface into a cylindrical one, which was due to a decrease in micropore volume.

Ponomarenko et al. [22] prepared SBA-15 silica samples in which pore shape factors ranged from 4539 to 9263, that is, from a slightly tortuous circular shape to a very corrugated. Then, the samples were used as templates for the preparation of carbon OMMs. The question arises - to what extent do the replicas F_{rep} inherit the F_{tem} shape of silica nanotubes ?

We found that the pores of the carbon replica are clustered around F_{rep} = 4500 (75% of circular), while the pores of their silica templates are grouped around F_{tem} = 8000. Based on the original and our calculated data, we can conclude that carbon, deposited inside silica, behaves like a compressed spring. After the silicate is dissolved, the carbon channels elongate (up to 2.5 ÷ 6.5 times), and their wall thickness becomes 2.0 ÷ 9.8 times thicker than that of silica; as a result, their shape becomes close to circular.

The same carbon behavior was observed in **Lee** al. [23] study. The matrix was 2D hexahonal mesoporous silica MSU-H, the carbon precursor was sucrose mixed with boric acid as an antifoam [6] and only variable; 7 samples were synthesized. In addition to S_{BET}, V_p and D_p, they mesured micropore volume $V_{<2\ nm}$. Our calculations showed that each m^2 of the surface area contains the same micropore volume, i.e., the $V_{<2\ nm}/S_{BET}$ ratio is 0.000425 cm^3/m^2 for all samples, STD = 1.03 %. Range F was 3175 ÷ 7123; F correlates with $V_{<2\ nm}$ only in low F range (3175 ÷ 4800), but there are clear inverse-proportional relationships in the entire range between F and ***t***/D_p (Fig.3) as well as between F and L_{si} (not shown), that is growth F with thinning and elongation the pore walls.

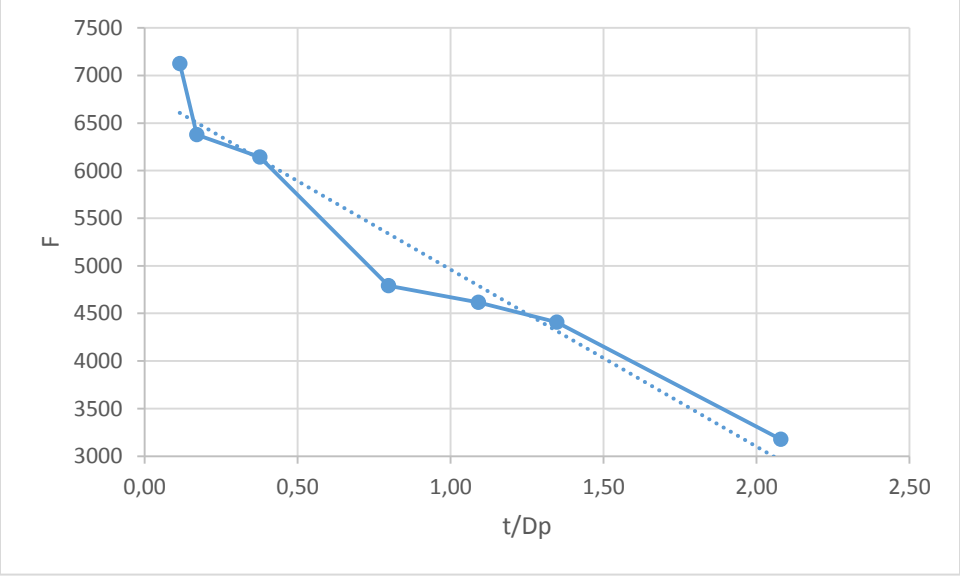

Fig 3: The effect of t/D_p (size effect) on pore shape factor F. Based on data from Lee et al. [23].

Gadiou et al. [24] prepared 5 samples of microporous AC as carbon replicas of the ordered patterns of mesaporous silica. AC was designed to store H_2. The processing variables were: i) SBA-15 and MCM-48 silica matrices, ii) carbon precurcors: pitch, sucrose and propylene. Carbon to silica ratio was almost equal for all 5 samples. The probing gases were: N_2 (shows the volume $V_{<2\ nm}$, i.e.volume of micropores with size < 2 nm), CO_2 (shows the volume $V \leq 1$ nm, i.e. volume of pores with size ≤ 1 nm) and H_2.

SBA-15 contains cylindrical mesopores connected through smaller pores. MSM-48 has a cubic structure formed by two complexly intertwined mesoporous channels: windows are formed by rib-walls of channels.

The AC pore surface area S_{BET}, average diameter D_p and, calculated by us, F and Lsi show that the carbon mass stretches after removing the silica template. The best H_2 storage was the replica CS48 (sucrose-MCM-48), it has the highest surface area, smallest pore diameter and, as a result, the longest surface length index L_{si}. Of the 5 samples, 4 had F 4400 ÷ 5400 and 1 - F = 7098. SBA-15 cylindrical mesopores provide a cylindrical – spherical (F ≈ 5000) shape of carbon replicas regardless on the carbon precursor. Inside the MCM-48, sucrose covers the surface of ribs, creating windows with close to the spherical shape (F = 5524), while the pitch is set primarily at the untersections of the ribs creating blocks and a complex corrugated pore system (F = 7098). A similar picture of the last sample was observed in our experiments with the deposition of a suspension of $Al(OH)_3$ inside the walls of alumina foam [25].

It was found again that regardless on the matrix and carbon precuror the value $V_{<2\ nm}$ per m^2 of surface area S_{BET} remainds constant, namely 0.0003 cm^3/m^2 with STD = 8.2 %. Common to these samples is material of the templates – silica. A similar ratio $V_{\leq 1\ nm}/S_{BET}$

fluctuates greatly, its STD = 43.8%. In the same time $V_{\leq 1\ nm}$ correlates with F in the range 4400 ÷5500 (Fig. 4); the transition of the pore shape from circular to spherical leads to the appearance the smallest pores (or vise versa).

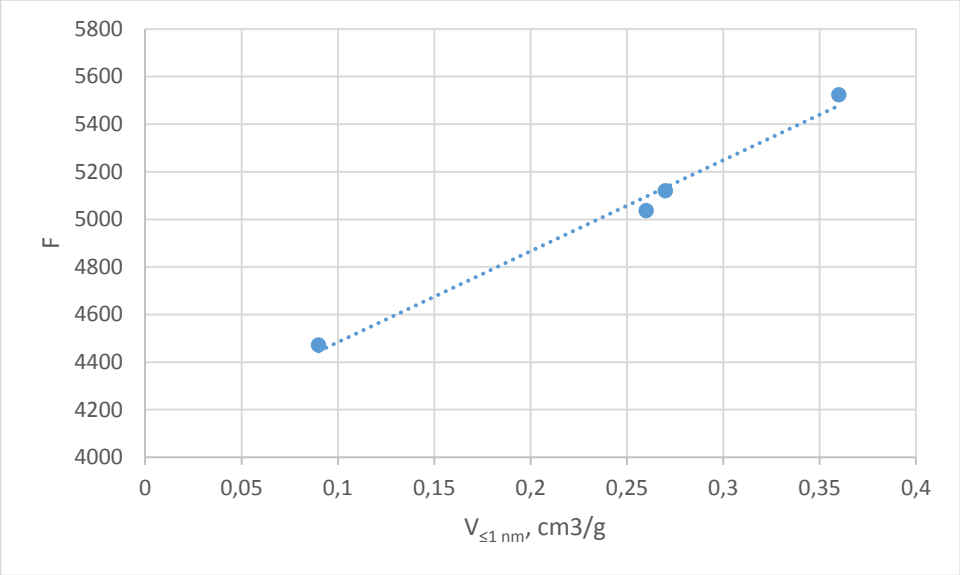

Fig.4: Effect of pore shape factor F on micropores < 1 nm volume (V_{CO2}). Based on data from Gadiou et al [24].

The point with maximal $V_{<1\ nm}$ and 50:50 % cylindrical – spherical pore shape (F = 5524) represents the best H_2 storage.

Bastos-Neto et al. [26] looked for commercial and non-commercial (random sampling) activated carbon (AC) as a methane storage; 10 samples were tested. The V_{mi} micropore volume was estimated from the N_2 adsorption - desorption isotherms by two methods: Dubinin-Radushkevitch (V_{miDR}) and Monte- Carlo molecular simulation (V_{miMC}).

The two methods gave very different V_{mi} values, so we checked the dependencies CH_4 uptake (mg/g) vs. both V_{mi} (cm^3/g). The DR method gave a cloud of points (no correlation), while the

MC method discovers that there are two series of samples (Fig.5) with clear direct dependences of CH_4 uptake on V_{miMC}.

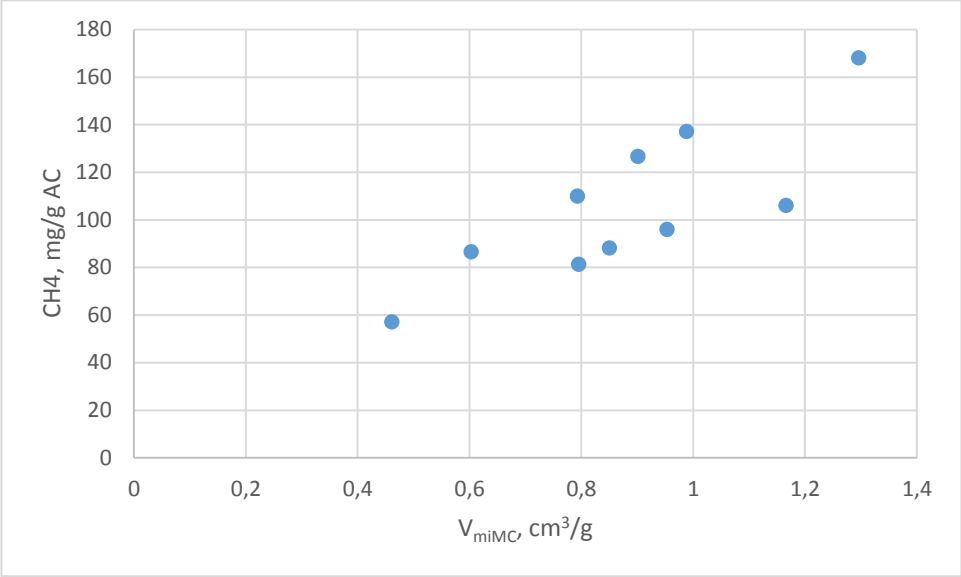

Fig 5: CH_4 uptake by AC vs. the micropore volume V_{miMC}. Based on data from [26].

There is a parameter (CH_4 uptake/$V_{<2\ nmMC}$), which is constant in each series: 104 mg/cm^3 (STD = 12%) for the right series and 138 mg/cm^3 (STD = 4%) for the left. Thus, there are parameters that are equal for samples within the series, but there is some parameter that separate them. No correlation of micropore volume with F (apparently because random sampling) exist, but CH_4 uptake is inversely proportional to F (excluding one sample with a maximum of F = 2453) (not shown). The ratio V_{miDR}/S_{BET} = 0.000509 cm^3/m^2 with STD = 19.3 %, while $V_{mi}MC/S_{BET}$ = 0.000593 cm^3/m^2 with STD = 26.2 %. STDs are significant, apparently due to random sampling.

Feng et al. [27] prepared CNTs as a carrier and Ni/CNTs as catalysts of CO_2 methanation. Acetonitryle (CNT-A) and methanol (CNT-E) were used as a carbon source; commercial both CNT (CNT-C) and AC were also been used (4 carriers and 4 catalysts). 12 wt

% Ni were highly dispersed on the carbon surface. CO_2 conversion rates were from 20% to 65%.

Using the presented S_{BET}, V_p and D_p, we found that all 8 carriers and catalysts have F-s = 3995 ÷ 4005, that is, “pure” circular pore shapes, therefore Ni deposition on carbon did not change their circular shape and smooth surface; so the difference in the activity of the samples cannot be explaned by F. At the same time, the conversion shows an increase with increasing particle size of Ni, which is unusual. The activity of the catalysts was explained by “the overflow effect of hydrogen for CNTs supports" [27]. So we started learn the CNTs.

The Ni/CNT parameters were recalculated per 1 g of CNT [27], that is, they were divided by 0.88 (minus 12 % of Ni), therefore in this case the “cat” index means carbon inside the catalyst. Then, the relationship between the catalyst/support ratios for S_{BET}, V_p, D_p and L_s of samples with % CO_2 conversion were checked. The most visible was the graph of % CO_2 conversion as a function of the ratio (L_s cat/L_s supp) (that is, depending on the stresses arising from the decrease in the length of the surface of the support after the introduction of Ni) is shown below (Fig. 6).

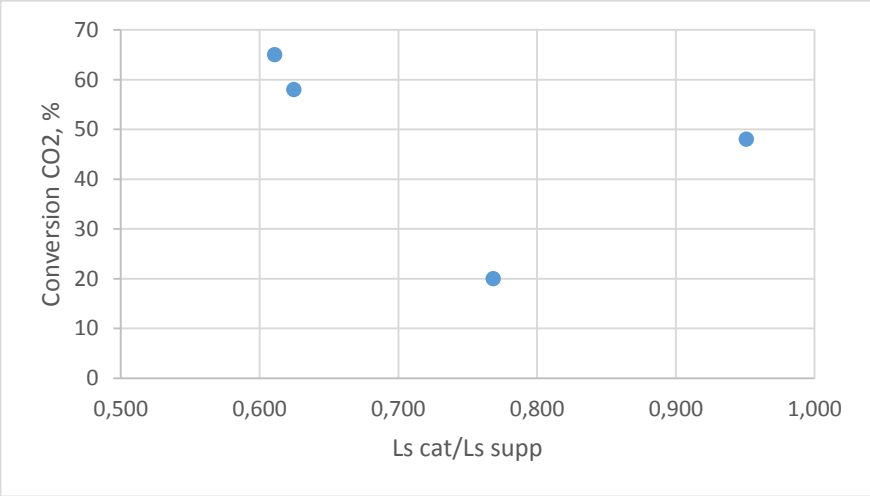

Fig. 6: CO_2 conversion dependence on activated carbone pore length reduction due to Ni incorporation. Supports AC, CNTs-A, CNTs-C and CNTs-E are placed in ascending order of CO_2 conversion. Based on data from Feng et al. [27].

Excluding the point (0.95; 48) that falls out of the dependence and represents Ni/CNTs-A (acetonitrile), one can see that the greater the compression of the carbon tube, the higher the reaction efficiency.

Zhang et al. [29] prepared 15 samples of activated carbon (AC) based on the hem stem; the processing variables were KOH/char ratio, activation temperature, and activation time. The reaction result was charactirized by AC yield. The best sample, having the largest specific surface area of 2388 m^2/g and a narrow pore size distributions, was obtained when the impregnation ratio was 4.5:1 (KOH/char), the activation temperature was 800^oC, and the activation time was 1.5 h. After calculating F and plotting the dependence of F on the Yield, %, (Fig. 7), we found that the *best* sample has the lowest F (3873), which corresponds to a *circular* pore shape.

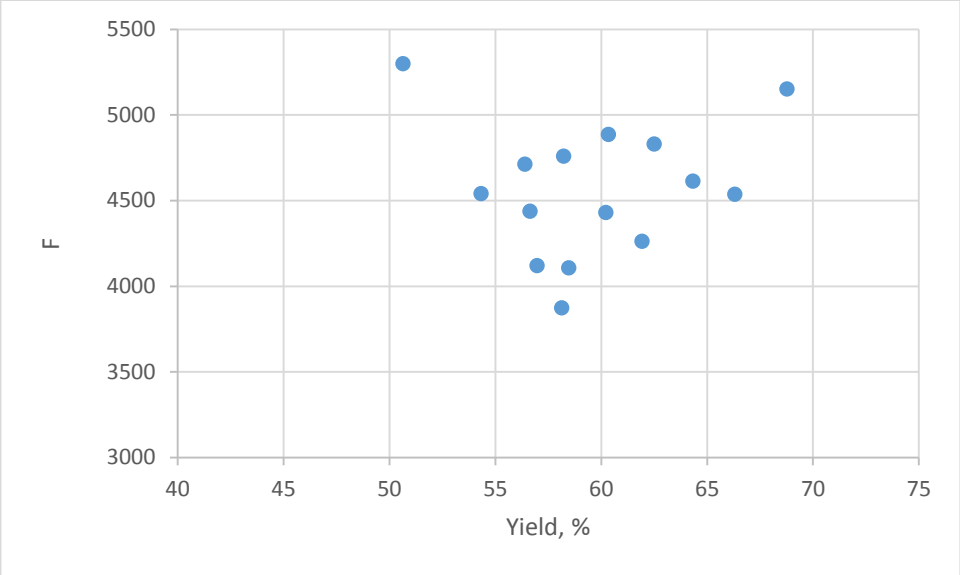

Fig.7: Activated carbon yield depending on pore shape F. Based on data from Zhang et al. [28].

Most samples are grouped around a point (60%, 4500). The parameter F separates the two extreme points of yield (51%; 5299 and 69 %; 5152), which are samples with a high spherical fraction of shapes.

Arshad et al. [29] used an empty fruit bunch as a raw material for the preparation of AC as a H_2 storage. The procedure includes a calcination of bunch in a stream of CO_2 followed by treatment with KOH solutions of 0.5M, 1M and 2M. SEM showed that all manufactured samples have cylindrical pores. Our calculations confirmed that all samples have F ≈ 4000, therefore V_{mi} cannot depend on F. Therefore, the pore length Ls [2] (not L index because F = 4000), S_{BET}, and V_p were tested as parameters affecting V_{mi} and S_{mi}.

All checked pairs showed direct proportional dependencies: an increase in KOH concentration led to a simultaneous increase in both D_p and L_{si} similarly to materials with a positive Poisson number. The V_{mi}/S_{BET} ratio is constant (0.00041 cm^3/m) with STD = 5 %.

Thielemann et al. [30] studied the effect of washing freshly prepared SBA-15 with water, ethanol, and mixtures thereof on the properties of SBA-15. Recently [2], we showed that ethanol blurs the mouths of intra-wall pores and converts part of these pores into open micropores.

It can now be shown (for the sample 3A) that an increase in the surface area of micropores leads to a decrease in spherical motifs and an increase in cylindrical (up to 25%) motifs of pore shape (Fig. 8).

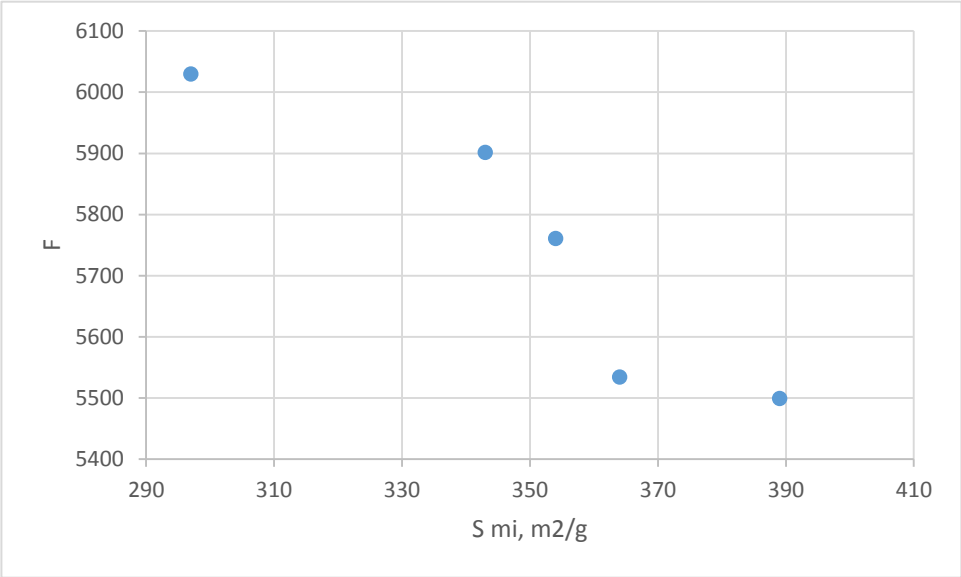

Fig. 8: The relationship between the surface area of micropores S_{mi} and the pore shape factor F as a result of washing freshly prepared SBA. Based on data from Thielemann et al. [30].

The constancy of the ratios $V_{<2\ nm}/S_{BET}$ (remark).

In the process of searching for the relationships between the shape of the pores and microporosity, another parameter was revealed that turned out to be constant. $V_{<2\ nm}/S_{BET}$ constancy was found in works of Zubizarreta et al. [18], Pagketanang et al. [21], Lee al. [23],

Gadiou et al. [24], and Arshad et al. [29]. The direct-proportional dependency of $V_{<2\ nm}$ on S_{BET} was demonstated by Emel'chenko et al. [33] for 7 samples mesoporous carbon nanostructures with the inverse opal lattice: $V_{<2\ nm}/S_{BET} = 0.000372\ cm^3/m^2$ (STD = 6.2 %). Alam and Mokaya [33] prepared 6 samples of microporous carbons using zeolite Y as template; we got $V_{<2\ nm}/S_{BET} = 0.000416\ cm^3/m^2$ (STD = 2.4 %).

We assume that this constancy indicates that both parameters are estimated from the same N_2 adsorption isotherms. A useful number is Standard Deviation (%) of $V_{<2\ nm}/S_{BET}$, which shows the homogeneity of the samples in the series. The smallest STD = 1.03 % was obtained for the released "compressed spring" of the active carbon replica in the Lee study [23].

Conclusion

Three new generalized texture parameters (GTP) of porous materials have been proposed. The pore shape factor F is dimensionless contineous parameter covering the total surface area, total pore volume and pore size in their entire range. Special cases are F of slit, circular and spherical pores. Change F manifests itself in the creation of new surface motifs which is accompanied by the appearance of stresses, deformations, new microporores or healing existing ones.

The $\boldsymbol{t}/D_p$ ratio, which was known as the parameter causing wall stresses in the radial direction, was transfered to the status of the generalized parameter, and now it is a regular texture parameter.

The $L_{si} = S_{BET}/D_p$ ratio, named the "surface length index", was proposed as parameter that causes stresses and wall deformations in the axial direction for pores of any shape.

All proposed GTPs provide a better understanding of the formation and behavior of porous materials. Carbon samples behavior similar to auxetic materials were discovered. For molecules of complex shapes, molecular sieving according to their shapes has been proposed and demonstrated.

Supporting information.

Supporting Information File 1. Calculations of new textural parameters for the CNF/MWCNT hybrid prepared by Jeong et al. [17].

Funding – the article was made without financial support.

https://www.researchgate.net/scientific-contributions/74443099_L_Titelman

References

1. Vradman L.; Titelman L.; Herscowitz M. *Micropor. Mesopor. Mater.* **2006**, *93*, 313-317. DOI:10.1016/j.micromeso.2006.03.014.

2. Titelman L. SN Appl. Sci. **2019**, *1*, 1294. https://doi.org/10.1007/s42452-019-1318-2.

3. Gibson F.J.; Ashby M.F. 1997 Cellular Solids: Structure and Properties, second ed., Cambridge **1997** Univ. Press, Cambridge, UK

4. Williford R.E.; Li X.S.; Addleman R.S.; Fryxell G.E.; Baskaran S.; Birnbaum J.C.; Coyle C.; Zemanian T.S.; Wang C.; Courtney A.R. Micropor. Mesopor. Mater. **2005**, *85*, *3*, 260-266. https://doi.org/10.1016/j.micromeso.2005.06.024

5. Sozer N.; Dogan H.; Kokini J. J. Agric. Food Chem., **2011**, *59*, 5, 1498-1507. https://doi.org/10.1021/jf103766x

6. Titelman L. Generalized processing-structural functions for porous materials. J Porous Mater. **2012,** *19*, 1-13. https://doi.org/10.1007/s10934-010-9440-y.

7. Titelman L.I.; Levitskaya N. A. Russian Journal of Applied Chemistry (Zhurnal Prikladnoi Khimii), **1987,** LX, *12*, 2666 – 2670 (in Russian).

8. Zukerman R.; Vradman L.; Titelman L.; Weidenthaler C.; Landau M.; Herskowitz M. Microp. Mesop Mater. **2008**, *116*, 237–245. doi:10.1016/j.micromeso.2008.04.011

9. Mohan M.; Sharma V.K.; E. Kumar A.; Gayathri V. Energy storage **2019**, *1* (2). https://doi.org/10.1002/est2.35

10. Pirngruber G (28 October ***2014***) Physisorption and pore size analysis. Characterization of porous solids - Surface Science and Catalysis Course – G. Pirngruber.

11. Galarneau A.; Abid Z.; Said B.; Didi Y.; Szymanska K.; Jarz¸ebski A.; Tancret F.; Hamaizi H.; Bengueddach A.; Di Renzo F.; Fajula F. Inorganics ***2016***, *4*, 9; 1-25. doi:10.3390/inorganics4020009.

12. Landau M.V.; Savilov S.V.; Ivanov A.S.; Lunin V.V.; Titelman L.; Koltypin Yu.; Gedanken A. J Mater Sci. **2011.** *46*(7), 2162 – 2178. DOI 10.1007/s10853-010-5053-8

13. García A.; Solano J.P.;Vicente P.G.; Viedma A. Appl. Thermal Eng. **2012,** *135*, 96-201. doi:10.1016/j.applthermaleng.2011.10.030

14. Aligizaki K.K. Pore Structure of Cement-Based Materials. Testing, interpretation and requirements. Abingdon [England], **2006**. 432 pp. New York : Taylor & Francis. https://doi.org/10.1201/9781482271959

15. Putz A-M.; Cecilia S.; Ianăşi C.; Dudás Z.; Székely K.; Plocek J.; Sfârloagă P.; Săcărescu L.; Almásy L. J. Porous Mater. **2015**, *22*, 321-331. https://doi.org/10.1007/s10934-014-9899-z

16. Moyseowicz A.; Sliwak A.; Gryglewicz G. J. Mater. Sci., **2016**, *51*(7), 3431-3439. https://doi.org/10.1007/s10853-015-9660-2

17. Jeong Y.; Lee K.; Kim K.; Kim S. Materials (Basel), **2016**, *9*(12): 995. PMCID: PMC5457023

18. Zubizarreta L.; Mene´ndez J.A.; Job N.; Marco-Lozar J.P.; Pirard J.P.; Pis J.J., (2010) Carbon **2010**, *48*, 2722 – 2733. doi:10.1016/j.carbon.2010.03.068

19. Serra E.; Mayoral A.; Sakamoto Y.; Blanco R.M.; Dı´az I. Micropor. Mesopor. Mater., **2008**, *114*, 201–213.

https://doi.org/10.1016/j.micromeso.2008.01.005

20. Landau M.V.; Titelman L.; Vradman L.; Wilson P. Chem Commun Camb), **2003**, Mar 7(5), 594-5. doi: 10.1039/b211585a.

21. Pagketanang T.; Artnaseaw A.; Wongwicha P.; Thabuot M. Energy Procedia, **2015**, *79*, 651 – 656. doi: 10.1016/j.egypro.2015.11.550

22. Ponomarenko I.; Parfenov V.; Zaitseva Yu.; Zharkov S.; Kirik S. Glass Physics and Chemistry, **2014**, *40*, No.1, 79–87. https://doi.org/10.1134/S1087659614010180

23. Lee H.I.; Kim J.H; You D.J.; Lee J.E.; Kim J.M.; Ahn W.S.; Pak C.; Joo S.H.; Chang H.; Seung D. Adv. Mater. **2008**, *20*, 757-762. DOI: 10.1002/adma.200702209

24. Gadiou R.; Saadallah S-E.; Piquero Th.; David P.; Parmentier Ju.; Vix-Guterl C. Micropor. Mesopor. Mater. **2005**, *79*, 121–128. doi:10.1016/j.micromeso.2004.10.034

25. Landau M.; Shter G.E.; Titelman L.; Gelman V.; Rotter H.; Grader G.S.; Herskowitz M. Ind. Eng. Chem. Res. **2006**, *45*, 7462-7469. https://doi.org/10.1021/ie0606744

26. Bastos-Neto M.; Canabrava D.V.; Torres A.E.B.; Rodriguez-Castellon E.; Jime´nez-Lo´pez A.; Azevedo D.C.S.; Cavalcante Jr. C.L. Appl. Surf. Sci., **2007,** *253*, 5721–5725. doi:10.1016/j.apsusc.2006.12.056.

27. Feng Ya.; Yang W.; Chu W. Int. J. Chem. Eng. **2015**. Article ID 795386, 7 pages. http://dx.doi.org/10.1155/2015/795386.

28. Vradman L.; Landau M.V.;, Kantorovich D.; Koltypin Y.; Gedanken A. Micropor. Mesopor. Mater. **2005**, *79*, 307–318. doi:10.1016/j.micromeso.2004.11.023

29. Zhang Ji.; Gao Ji.; Chen Yao; Hao Xi.; Jin Xi. Results in Physics, **2017**, *7*, 1628-1633. https://doi.org/10.1016/j.rinp.2017.04.028

30. Arshad S.H.Md.; Ngadi N.; Aziz A.A.; Amin N.S.; Jusoh M.; Wong S. J. Energy Storoge. **2016**, *8*, 257–26. http://dx.doi.org/10.1016/j.est.2016.10.001

31. Thielemann J.; Girgsdies F.; Schlögl1 R.; Hess C. Beilstein J. Nanotechnol. **2011**, *2*, 110-118. doi:10.3762/bjnano.2.13

32. Emel'chenko G.A.; Masalov V.M.; Zhokhov A.A.; Khodos I.I. Phys. Solid State, **2013**, *55*, 1105–1110 (2013). https://doi.org/10.1134/S1063783413050090

33. Alam N.; Mokaya R. Energy Environ. Sci., **2010**, *3*, 1773–1781. DOI: 10.1039/c0ee00154f

Acknowledgements – The author is grateful to the researchers, whose experimental data were used to demonstrate the new dependences.